Patch-Based Super-Resolution of Arterial Spin Labeling Magnetic Resonance Images

Cédric Meurée, Pierre Maurel, Jean-Christophe Ferré, Christian Barillot

▶ **To cite this version:**

HAL Id: inserm-01880726
https://inserm.hal.science/inserm-01880726v2

Submitted on 25 Feb 2019

Patch-Based Super-Resolution of Arterial Spin Labeling Magnetic Resonance Images

Cédric Meurée [1,2], Pierre Maurel[2], Jean-Christophe Ferré[2,3], Christian Barillot[2]

[1] *Siemens Healthcare SAS, Saint-Denis, France*
[2] *Univ Rennes, CNRS, Inria, Inserm, IRISA UMR 6074, VISAGES - ERL U 1228, F-35000 Rennes, France*
[3] *CHU Rennes, Department of Neuroradiology, F-35033 Rennes, France*

Abstract

Arterial spin labeling is a magnetic resonance perfusion imaging technique that, while providing results comparable to methods currently considered as more standard concerning the quantification of the cerebral blood flow, is subject to limitations related to its low signal-to-noise ratio and low resolution. In this work, we investigate the relevance of using a non-local patch-based super-resolution method driven by a high resolution structural image to increase the level of details in arterial spin labeling images. This method is evaluated by comparison with other image dimension increasing techniques on a simulated dataset, on images of healthy subjects and on images of subjects scanned for brain tumors, who had a dynamic susceptibility contrast acquisition. The influence of an increase of ASL images resolution on partial volume effects is also investigated in this work.

Keywords: MRI, Arterial Spin Labeling, Super-Resolution, Denoising, Partial Volume Effects

1. Introduction

Cerebral perfusion corresponds to the delivery of nutrients and oxygen to brain tissues. Its assessment is important for clinicians, as it has been shown that abnormal perfusion patterns are often the causes or consequences of pathologies [1].

Arterial spin labeling (ASL) is a non-invasive magnetic resonance (MR) imaging technique that quantitatively evaluates this perfusion. Radio frequency

inversion pulses are applied to the blood water protons flowing through the neck of the imaged subject. After a certain amount of time left for these labeled protons to reach the brain, called the post-labeling delay (PLD), an image is acquired, which is called the labeled image. The difference between this image and a control image, acquired without the labeling step, is proportional to brain perfusion. The cerebral blood flow (CBF) can be quantified from this perfusion image [2, 3]. Recommendations regarding ASL image acquisitions have been formulated by a consortium in the ASL "white paper" [4].

While very promising in some aspects, ASL is, however, still subject to a number of limitations. Indeed, fast acquisition techniques such as echo planar imaging (EPI) are required to image the dynamic process of the labeled protons circulation, which generate low resolution and low signal-to-noise ratio (SNR) images. For that reason, multiple label and control pairs are usually acquired and averaged. However, this makes ASL subject to new potential corruptions, such as movement artifacts and the introduction of outlier intensity values. Moreover, voxelwise estimations of perfusion related parameters are corrupted by small subject motion and the low resolution of the images, that involve the introduction of partial volume effects (PVE), meaning that perfusion of different tissues contribute to the perfusion signal observed in a single image voxel [5, 6, 7].

Several post-processing algorithms have been proposed to deal with these limitations. Particularly, denoising methods are successfully applied to deal with artifacts and outliers in ASL images [8, 9, 10, 11]. PVE correction algorithms have also been proposed and investigated in [6, 7, 12]. These methods have in common to be applied at the resolution of the acquired images. While attenuating the effect of the previously listed corruptions, they do not allow to increase the level of details in images. However, this aspect could be of great interest, the thickness of grey matter (GM) being often inferior to the size of the ASL images voxel size. In clinical conditions, acquiring ASL images at higher resolutions is a challenging task, since this would imply a decrease in SNR, or increase the acquisition time.

Various methods have been proposed in order to increase the resolution of MR images facing similar low resolution properties, such as T2-weighted and diffusion images, as a post-processing step. Interpolation methods can be applied to MR images (trilinear interpolation, B-splines), unfortunately resulting in blurred images. To overcome this aspect, super-resolution (SR) approaches allow to reconstruct high frequency information from low reso-

2

lution data. Some of these methods are based on multiple low resolution acquisitions, therefore requiring specific acquisition protocols, which can be time consuming [13]. Recently, [14, 15, 16] have adapted and extended non-local patch-based SR approaches that are independent of the acquisition process to the MRI domain. The main idea consists in using self similarities in the images to perform reconstructions at higher resolutions [17]. These methods can be applied to data commonly acquired in clinical conditions, such as T2-weighted or diffusion weighted images, thus preventing any increase in the acquisition time. A first application of this kind of method to pseudo-continuous ASL (pCASL) images has been proposed in [18]. The main limitation of these methods is that they require clean low resolution data as inputs, which means that denoising algorithms must first carefully be applied to the images prior to SR reconstruction.

In this paper, we propose a novel method to increase the resolution of ASL images, which deals with the presence of noise. This non-local patch-based SR reconstruction approach is based on the assumption of appearing similarities between neighborhoods in the image that is reconstructed and a high resolution (HR) structural image, generally acquired in imaging protocols. This assumption of shared anatomical properties between structural and ASL images comes from the fact that gray matter and white matter are the two tissues that contribute to the brain ASL signal, with their own perfusion characteristics (e.g. CBF and arterial arrival time) [6, 7, 12]. This proposition allows to increase the resolution of ASL images without extending the acquisition time. The method is evaluated on a simulated dataset and images of healthy subjects in order to investigate its capacity to reconstruct images close to HR ASL references. As DSC is commonly considered as a reference perfusion imaging technique, we investigate the ability of our method to generate images closer to the DSC quantitative maps on images acquired on subjects scanned for brain tumors. In addition, we investigate the influence of a recovery of HR details on PVE.

The material and methods are presented in section 2, results regarding comparisons between generated images and reference HR ASL or DSC maps in section 3, an evaluation of the influence of the SR reconstruction on PVE in section 4 and a discussion of these aspects in section 5.

3

2. Materials and Methods

2.1. Summary of existing similarity-based SR methods

The objective of super-resolution methods is to recover an unknown high resolution (HR) image x from a low resolution acquired one y. The following model explicits the relation between both images :

$$y = Mx + \eta, \tag{1}$$

with M a matrix representing subsampling, blurring and geometric transformations, and η representing some additive noise [17, 14, 15, 16]. An optimization problem of the following form would correspond to a common approach to recover the unknown image x:

$$\tilde{X} = \arg\min_x \{ \left\| y - Mx \right\|_2^2 + \gamma \Phi(x) \}, \tag{2}$$

where Φ is a regularization term necessary to solve this ill-posed minimization problem and γ a positive parameter.
As shown in [15] and [16], an iterative reconstruction-correction procedure can be adopted in order to reconstruct x, which allows to avoid problems such as local minima or parameters initialization linked to this ill-posed optimization problem. This procedure consists in two steps, corresponding to a reconstruction and a subsampling consistency constraint.
The reconstruction is based on the assumption that locations in a HR acquired structural image and the SR reconstructed one should share anatomical properties, and that the structural image could therefore be used to drive the reconstruction process. This assumption leads to the choice of non-local regularization approaches, such as in [15] and [16].
The subsampling consistency imposes the constraint of a strict equality between the downsampled version of the SR reconstructed image and the original low resolution image y, which is made possible by formulating strong assumptions about the M matrix composition. However, this constraint implies the need for well denoised low resolution images for the method to be consistent. Therefore, Coupé et al. [16] proposed to apply a Rician-adapted denoising filter on diffusion images before solving the optimization problem. In the case of low signal-to-noise ratio ASL images, different noise patterns can be introduced regarding the scanners, sequences or settings chosen to perform the acquisition. The use of parameters that could not be the most appropriate ones in the filtering step, could have important consequences

4

regarding the quality of the final reconstructed image. This is the reason why we introduce a reconstruction driven by a HR structural image, while denoising the SR reconstructed image at the same time.

2.2. A new SR method for ASL images

The main objective of this work is to assess the relevance of using a HR anatomical image to increase the resolution of ASL images. Following a similar idea than [14], [15] and [16], we propose a non-local patch-based method, while introducing a novel denoising strategy.

Because of the use of non-local patch-based approaches, both in the denoising and SR methods previously described [16], we propose to combine them in a unique SR image reconstruction process. A third order B-splines interpolation is first applied to the low resolution image in order to increase its dimension to the desired one. This initialization is followed by iterations between a non-local patch-based regularization and a fidelity term assuring the global intensities mean consistency between the initial low resolution image and the reconstructed one. This fidelity term differs from the one in use in the works presented in the previous section [15, 16], in the sense that it involves a global image mean consistency, and not a subsampling consistency at the voxel level, therefore allowing a denoising of the reconstructed image. In the regularization term, correspondences between voxels' neighborhoods are assessed both in the reconstructed image and the structural one:

$$X_i^{t+1} = \frac{1}{Z_i} \sum_{j \in V_i} X_j^t \exp - \left(\frac{||N(X_{i,S}) - N(X_{j,S})||_2^2}{\beta_{struct}\sigma_{i,S}^2} + \frac{||N(X_i^t) - N(X_j^t)||_2^2}{\beta_{asl}\sigma_i^2} \right),$$
(3)

where X_i^t is the intensity of voxel i in the image X^t corresponding to iteration t, X_S the structural image, $N(X_i)$ and $N(X_{i,S})$ patches selected around voxel i in the ASL and structural images respectively, σ_i^2 and $\sigma_{i,S}^2$ the empirical local variances, V_i the correspondence search volume around voxel i, Z_i a scaling parameter controlling that the sum of the weights is equal to 1, and β_{asl} and β_{struct} two scalars adjusting the importance of the terms related to the ASL and structural images. The exponential weights, including an evaluation of the simultaneous similarity of voxel neighborhoods in the structural HR and reconstructed images, enable an increase in the level of details in the ASL image, while preserving features that are only visible in this image. Indeed, if neighborhoods are similar on two voxel locations in both images,

5

the contribution in the regularization will be important. In the contrary, if a feature is only visible in one of the images, the weight will have a lower value, and have a reduced contribution in this process.

The global low resolution mean value consistency corresponds to an additive offset equal to the difference between the mean image value of X^t and the mean of the low resolution image Y, respectively $\mu(X)$ and $\mu(Y)$:

$$X^{t\prime} = X^t + \big(\mu(Y) - \mu(X^t)\big). \tag{4}$$

Iterations between these two steps are performed until no significant difference between consecutive reconstructed images can be observed, which can be written as follows:

$$\frac{|X^{t-1} - X^{t-2}|}{|X^t - X^{t-1}|} < \tau. \tag{5}$$

As in [16], a coarse to fine approach is proposed where the weights β_{asl} and β_{struct} are decreased at each iteration of the process, leading to $[\beta_{asl}, \beta_{asl}/2, \beta_{asl}/4, ...]$ and $[\beta_{struct}, \beta_{struct}/2, \beta_{struct}/4, ...]$ respectively.

2.3. Validation framework

2.3.1. Simulated dataset

In order to evaluate the proposed method in a controlled environment, we constructed a simulated set of 9 CBF maps. This dataset was built from structural (MP2RAGE UNI, [19]) images acquired at a resolution of $1 \times 1 \times 1$ mm^3 with a 3T Siemens Verio scanner and a 32-channel head-coil. Fixed CBF values were considered for gray matter (GM) and white matter (WM), equal to 70 and 25 ml/100g/min respectively [20]. These values were affected to the probability maps obtained by means of the SPM12 segmentation algorithm [21], leading to the application of the following equation:

$$\text{cbf}_i = p_{GM,i}.70 + p_{WM,i}.25, \tag{6}$$

with cbf$_i$ the simulated CBF value at voxel i, and $p_{GM,i}$ and $p_{WM,i}$ the respective partial volume probability values for GM and WM provided by the segmentation at the same voxel location.

These HR simulated CBF maps were then downsampled to a resolution of $2 \times 2 \times 2$ mm^3 by applying a gaussian blurring before downscaling by a factor of 2 in the 3 directions. The downsampled images were then reconstructed at the original resolution using the proposed SR reconstruction method. In

order to assess the influence of the ASL and structural related terms on the proposed reconstruction, implementations with different β_{asl} and β_{struct} values were evaluated. Images reconstructed by only taking the ASL or the structural related term into account were generated. β_{asl} and β_{struct} pairs equal to [0.25; 0.75], [0.5; 0.5] and [0.75; 0.25] were also evaluated. Images reconstructed by means of nearest neighbor interpolation, trilinear interpolation and 3rd order B-splines interpolation were then generated and compared to the CBF maps reconstructed by means of the proposed method performed with the selected β_{asl} and β_{struct}.
The root mean square errors (RMSE) between the original HR simulated CBF maps and the reconstructed images were calculated in order to evaluate the ability of each method to provide reconstructed images close to this reference.
As ASL images acquired in clinical conditions are usually affected by noise, commonly considered as gaussian in CBF maps due to the averaging of multiple label-control pairs, we also studied the behavior of each of these methods as a function of the amount of noise. Downsampled images affected by gaussian noise with standard errors corresponding to 3 to 14% of the GM CBF value were reconstructed at the original resolution in order to evaluate this behavior. Figure 1 illustrates these images generation and the processing steps.

2.3.2. Healthy controls

The SR reconstruction method was also evaluated on images acquired on 4 healthy subjects (3 females, 1 male, age = 34 ± 6 years). For each of these volunteers, images were acquired on a 3T Siemens Verio scanner with a 32-channel head-coil. The structural image was a MP2RAGE UNI (resolution: $1 \times 1 \times 1$ mm^3). pCASL (resolution: $3.5 \times 3.5 \times 5$ mm^3, interslice gap: 1 mm, 30 control-label pairs repetitions, PLD: 1800 ms, labeling duration (LD): 1800 ms, 20 slices [22]) and M0 (resolution: $3.5 \times 3.5 \times 5$ mm^3, interslice gap: 1 mm, 5 repetitions, 20 slices) images were acquired as the low resolution data used to generate the CBF maps to be reconstructed by increasing their dimensions by a factor of 2 in each direction. HR pCASL images were also acquired for the evaluation purpose (resolution: $1.75 \times 1.75 \times 2.5$ mm^3, interslice gap: 0.5 mm, 100 control-label pairs repetitions, PLD: 1800 ms, LD: 1800 ms, 20 slices), as well as HR M0 (resolution: $1.75 \times 1.75 \times 2.5$ mm^3, interslice gap: 0.5 mm, 10 repetitions, 20 slices). While not allowing to cover the entire brain, a number of 20 slices was selected for these HR acquisitions
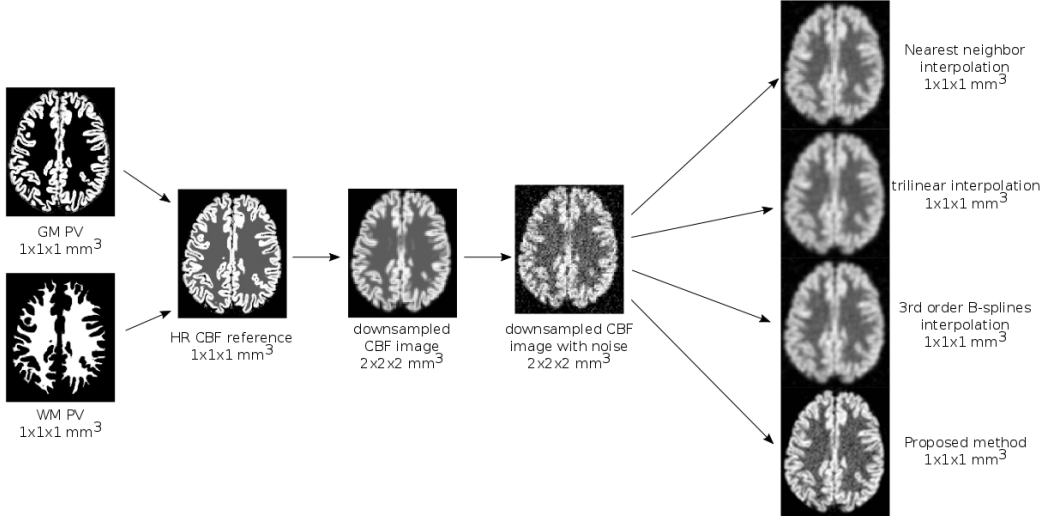
Figure 1: Pipeline describing the generation of the simulated dataset and the different reconstruction methods to be compared, applied to the downscaled and noise corrupted images.

as a matter of acquisition time. Image SNR being proportional to voxel volume, 100 repetitions were acquired in order to generate the HR pCASL images. While not entirely compensating for the SNR decrease in comparison with the 30 repetitions low resolution acquisitions, this repetition number was chosen as a compromise between scan time (10 minutes), risk of subjects motion and SNR.

CBF maps were obtained by applying the general kinetic model for pCASL acquisitions [2]:

$$CBF = \frac{6000.\lambda.\Delta M.\exp(\frac{PLD}{T_{1,blood}})}{2.\alpha.T_{1,blood}.M0.(1 - \exp(-\frac{LD}{T_{1,blood}}))}, \tag{7}$$

with λ the blood/brain partition coefficient ($\lambda : 0.9$), α the labeling efficiency ($\alpha : 0.85$), ΔM the control-label difference, and $T_{1,blood}$ the blood T_1 relaxation time ($T_{1,blood} : 1650$ ms).
As in the case of the simulated data, RMSE values between the reconstructed images generated by the different methods and the HR pCASL CBF map, considered as the reference, were calculated.

8

2.3.3. Correlation with DSC

As mentioned in the introduction, Dynamic Susceptibility Contrast (DSC) imaging is often considered as a standard perfusion MR imaging technique. A contrast agent, usually gadolinium-based, is injected to the subject and the induced susceptibility effects are imaged via T2*-weighted acquisitions. In clinical conditions, this technique enables acquisitions at a higher resolution than ASL scans. Therefore, we studied the correlation between low resolution CBF maps obtained from pulsed ASL (PASL) images, the same images after an increase of the dimensions by a factor of 2 in each direction with different interpolation methods and the HR DSC CBF images.
The dataset contains images of 10 patients imaged for brain tumors (3 females, 7 males, age = 63 ± 13 years, 5 grade IV tumors, 1 grade III, and 3 patients not showing hyper-perfusion signals after evaluation by an experienced neuroradiologist). Images were acquired on a 3T Siemens Verio scanner with a 32-channel head-coil. A 3D T1w sequence (resolution: $1 \times 1 \times 1$ mm^3) was acquired, as well as a PICORE Q2TIPS PASL sequence with flow crusher gradients (EPI readout, TR: 3000 ms, TE: 18 ms, FOV: 192×192 mm^2, flip angle: 90°, in plane resolution: 3×3mm^2, slice thickness: 7 mm, interslice gap: 0.7 mm, inversion time (TI): 1700 ms, bolus width (TI_1): 700 ms, 30 control-label repetitions) and a DSC sequence (GRE EPI readout, TR: 1500 ms, TE: 300 ms, FOV: 230×230 mm^2, flip angle: 90°, in plane resolution:1.8×1.8 mm^2, slice thickness: 4 mm, interslice gap: 1.2 mm, 100 measures).

The CBF maps were generated from the DSC images by use of the MR manufacturer software. An arterial input function was manually chosen to calculate the DSC relative CBF on a voxel basis. The method in use is based on a singular value decomposition deconvolution, as described in Østergaard et al. [23]. The general kinetic model for PASL acquisitions was applied to the ASL scans [2]:

$$CBF = \frac{6000.\lambda.\Delta M.\exp(\frac{TI}{T_{1,blood}})}{2.\alpha.TI_1.M0}, \tag{8}$$

The other parameters are the same as in (7), except $\alpha : 0.98$.

Although linear correlation between ASL and DSC relative CBF has not been strictly demonstrated, in a first approximation as shown in [24, 25, 26], we assume that positive correlations should be obtained between both

9

estimations. Therefore, the Pearson correlation coefficients were calculated between the low resolution ASL CBF and the registered HR DSC CBF maps, and the SR reconstructed ASL CBF and DSC CBF maps.

2.4. Implementation details

An in-house image processing pipeline based on Python, Cython, Nipype [27] and SPM12 functions was used to conduct the experiments. Considering results presented in [16] and our own experiments, the patch size was chosen equal to $3 \times 3 \times 3$ voxels in the non-local patched-based regularization, and the search volume to $7 \times 7 \times 7$ voxels.

3. Results

3.1. Simulated dataset

Figure 2 presents the mean RMSE values obtained between the high resolution simulated references and the images reconstructed by means of the proposed SR reconstruction method for noise levels equal to 3%, 6% and 9% of the GM CBF value. One can first notice that referring to only one of the ASL or structural images provides less satisfactory reconstructions. Indeed, taking only the ASL image into account does not allow to recover details absent from the downsampled CBF maps. In the contrary, a reconstruction only based on the structural image will not allow to consider and preserve CBF patterns only visible in the ASL image. One can then notice that the balance between β_{asl} and β_{struct} does not lead to significant differences when a low level of noise is added to the simulated CBF maps. However, differences in this balance have a higher influence on the quality of the reconstruction when dealing with images corrupted by a higher noise level. In the case of $[\beta_{asl}; \beta_{struct}] = [0.25; 0.75]$, the weights generated to perform the reconstruction are more governed by the ASL related term, which can explain the higher RMSE values obtained when the level of noise increases. $[\beta_{asl}; \beta_{struct}] = [0.5; 0.5]$ and $[0.75; 0.25]$ provide lower RMSE values when a realistic noise level is added to the images, and no significant difference between their RMSE distributions can be noted. Therefore, in the context of this work, we propose to keep an equal contribution of the ASL and structural related terms, meaning $[\beta_{asl}; \beta_{struct}] = [0.5; 0.5]$.
Images corresponding to reconstructions of a low resolution CBF map corrupted by gaussian noise with a standard deviation equal to 9% of the GM CBF value, which we qualitatively suppose being a close example to effective

10

low resolution acquired images, are displayed in Figure 3. The images generated by use of interpolation techniques (nearest neighbor, trilinear and 3rd order B-spline interpolations) appear flattened, compared to the SR reconstructed map, which enables to recover sharp structures and edges. Table 1 confirms these observations, with lower mean RMSE values (in bold) calculated between the simulated reference images and the SR reconstructed ones than between the references and the interpolated images. In addition, the evolution of these RMSE values indicates that the more the standard deviation of noise increases, the closer to the reference the reconstructed image is in comparison with the interpolated images. This result is associated with the capability of the proposed method to denoise the images. Significant RMSE distribution differences between the proposed reconstruction method and all interpolation techniques are found for levels of noise superior to 9% of the GM CBF value (p<0.00111 after Bonferroni correction for an α level equal to 0.01), and are marked by asterisks in table 1.
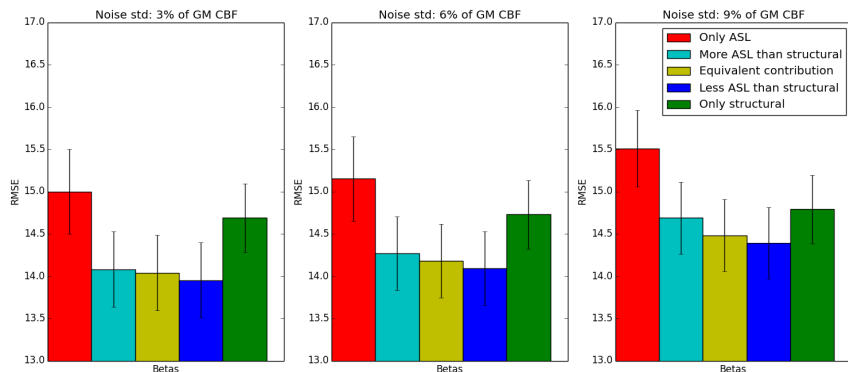

Figure 2: Graphs showing the RMSE values calculated between the reference HR image and images reconstructed with the proposed high resolution reconstruction method, by taking only the ASL, $[\beta_{asl}; \beta_{struct}]$ equal to [0.25; 0.75] (more ASL than structural), [0.5; 0.5] (equivalent contribution), [0.75; 0.25] (less ASL than structural), or only the structural image into account. The displayed noise levels correspond to 3%, 6% and 9% of the GM CBF value.

3.2. Healthy controls

Figures 4, and 5 present the images obtained from one of the 4 volunteers. Sagittal slices are shown, notably to insist on the influence of the methods on

11

Noise std	3	6	9	11	14
Nearest neighbor	$14.82 \pm 0.82^*$	$15.3 \pm 0.78^*$	$16.31 \pm 0.80^*$	$17.72 \pm 0.97^*$	$19.98 \pm 1.43^*$
Trilinear	$14.80 \pm 0.91^*$	$14.93 \pm 0.90^*$	$15.22 \pm 0.89^*$	$15.66 \pm 0.86^*$	$16.38 \pm 0.94^*$
B-splines	14.01 ± 0.89	14.35 ± 0.86	$15.08 \pm 0.83^*$	$16.12 \pm 0.85^*$	$17.78 \pm 1.19^*$
Proposed method	**13.92** ±1.05	**14.05** ±1.04	**14.34** ±1.01	**14.79** ±0.99	**15.56** ±1.08

Table 1: Means and standard deviations of the 9 RMSE values calculated between the reference HR image and the images reconstructed with nearest neighbor interpolation, trilinear interpolation, 3rd order B-splines interpolation and the proposed SR reconstruction method, with increasing levels of noise. Standard deviations of noise are expressed as percentage of the GM CBF value. Asterisks are joined to RMSE values corresponding to significant differences compared to the values obtained by application of the proposed method.

the staircase effect related to the particularly low initial resolution in the slice acquisition direction (5mm + 1mm gap). This effect is strongly corrected by the proposed SR reconstruction method. The RMSE values are reported in table 2, the proposed method providing images closer to the HR references than common interpolation techniques for three of the four subjects.

Method	Subject 1	Subject 2	Subject 3	Subject 4
Nearest neighbor	28.16	26.83	32.19	24.23
Trilinear	26.93	24.80	30.15	22.58
3rd order B-splines	**26.34**	25.04	29.68	22.49
Proposed method	26.44	**24.49**	**29.12**	**22.20**

Table 2: RMSE values calculated between the HR acquired reference image and the images generated by nearest neighbor interpolation, trilinear interpolation, 3rd order B-splines interpolation and the proposed SR reconstruction method, for each of the 4 healthy subjects (lower RMSE value in bold for each subject).

3.3. Comparison with DSC

Figure 6 reports, for each of the subjects, the values of the Pearson correlation coefficients obtained between the reference DSC CBF images and the low resolution acquired ASL CBF maps, their interpolations by trilinear and 3rd order B-splines and the images generated with the proposed SR reconstruction method. For each subject, the reconstructed image was more correlated to the DSC reference than the others. The significance of the differences was assessed by applying a Fisher transformation to the correlation
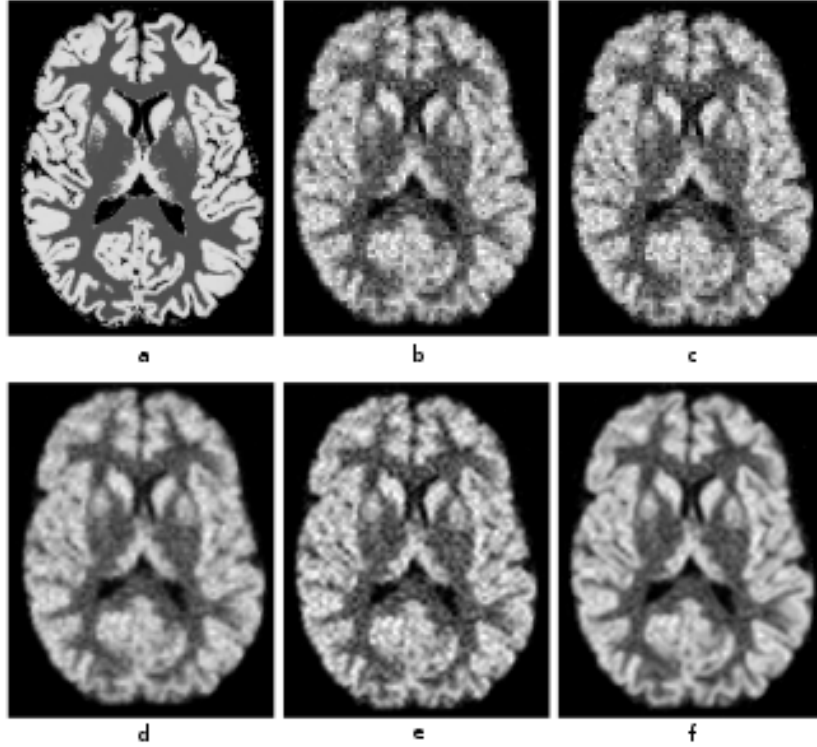
Figure 3: Simulated dataset: comparison of a) a HR reference image and b) the corresponding low resolution downsampled image corrupted by noise with std=9% of the GM CBF value, c) nearest neighbor interpolation, d) trilinear interpolation, e) 3rd order B-splines interpolation, and f) proposed SR reconstruction.

coefficients. The p-values obtained after this transformation indicate a significant difference between the correlation coefficients distributions. Indeed, a paired t-test between the correlation values obtained for the proposed reconstructions and the low resolution acquisitions provided a p-value equal to 1.4×10^{-4}, $p = 8 \times 10^{-5}$ by comparison with the trilinear interpolation, and $p = 3.33 \times 10^{-4}$ by comparison with the 3rd order B-splines. Figure 7 displays the DSC CBF images, low resolution ASL CBF maps and CBF maps reconstructed with our method for two of the patients.
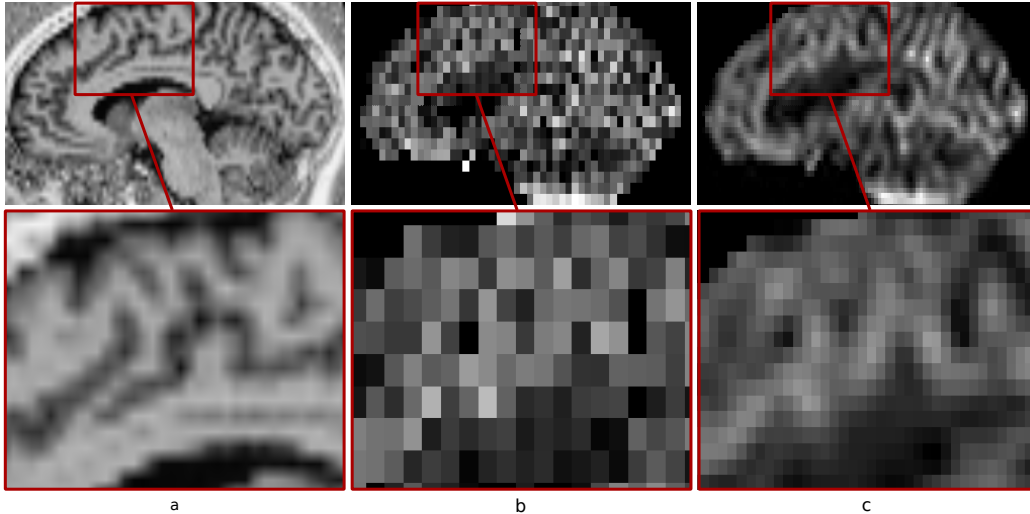
Figure 4: Healthy subject: sagittal slices of a) a structural image, b) the corresponding CBF map from the low resolution pCASL acquisition, and c) the proposed SR reconstruction. Upper line: sagittal slice, bottom line: zoom on the same slices.

4. Comparison with Partial Volume Correction methods

4.1. Method

Typical low resolution ASL acquisitions lead to well known PVE in ASL images, sometimes unfortunately preventing clinicians to interpret MRI observations such as reduced CBF values in regions of interest. Indeed, they could be the consequences of an effective reduced perfusion, a thinner GM or small subject motion. Because of the fact that the method described in this paper enables the recovery of high frequency details that are not visible in low resolution acquisitions, we propose to evaluate the influence of this recovery on a potential reduction of PVE. This is of particular interest, since the PVE correction methods that are currently the most commonly applied to ASL images correct CBF values at the voxel level, thus not providing better detailed images. Moreover, the method that we present in this work is only dependent on the registration of a HR structural image on an interpolated ASL one, while classical PVE correction methods require the use of tissue partial volume estimates. These partial volume estimate maps are provided by segmentation algorithms, and are therefore subject to potential additional errors.

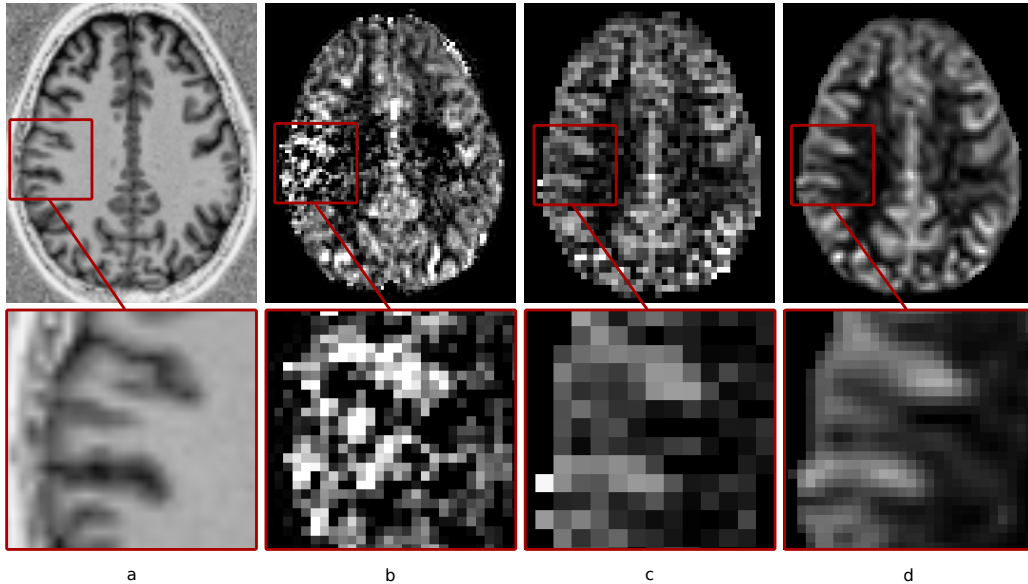In order to compare the impact of these algorithms on PVE, a simulation was

14

Figure 5: Healthy subject: axial slices of a) a structural image, b) the corresponding CBF maps from the acquired HR pCASL and c) low resolution pCASL acquisitions, and d) the proposed SR reconstructed CBF image. Upper line: sagittal slice, bottom line: zoom on the same slices.

conducted from the same 9 structural images as presented in 2.3.1, in which we aimed at having the most possible information about intensity values. In order to construct these 9 HR ASL images in which we knew the exact voxel constitution and associated values, images containing 100% GM or WM voxels were created, by thresholding the partial volume estimates generated by the SPM12 segmentation algorithm. Perfusion maps were generated by affecting ΔM values of 10 for GM and 1.5 for WM, with additional sinusoidal variations of 20% amplitude to make them more realistic, and evaluate the capability of the tested algorithms to preserve spatial variations and details [28]. The same process was used to create M0 images, with values of 1350 and 1000 in GM and WM respectively. These HR perfusion and M0 maps were downsampled by averaging $2 \times 2 \times 2$ voxel cubes, therefore reducing the size of the images and adding PVE, while knowing the exact brain tissue mixture of these new low resolution voxels. Different amount of gaussian noise (SNR=5,10) were added to these images in order to evaluate the influence of noise on PVE correction. The general kinetic model for pCASL acquisitions was then applied to obtain the corresponding CBF maps ($\lambda : 0.9$, $\alpha : 0.85$,
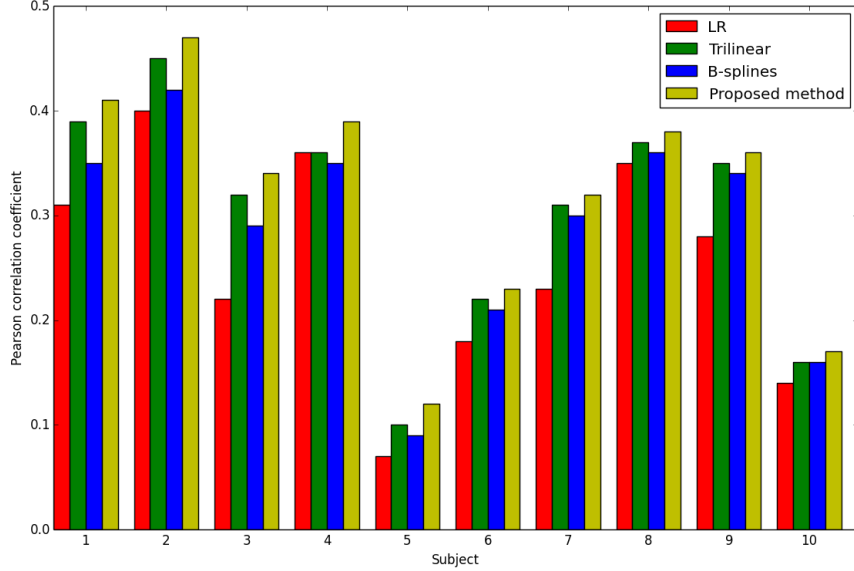
15

Figure 6: Pearson correlation coefficient between the reference DSC CBF maps and low resolution CBF images, the same images after trilinear interpolation, 3rd order B-splines interpolation and the proposed SR reconstruction method. These coefficients are presented for each of the 10 subjects.

369 $T_{1,blood}$: 1650 ms, LD: 1800 ms, PLD: 1800 ms).

370 The effect of the proposed algorithm on PVE was evaluated by analyzing its
371 ability to recover the effective GM contribution in the CBF values observed
372 in each voxel, in comparison with the linear regression method, which is one
373 of the standard PVE correction technique applied to ASL images [6].
374 Our proposed SR method provides high resolution CBF maps unlike the lin-
375 ear regression method, which produces two partial volume maps at the initial
376 resolution. This is the reason why our SR CBF maps have been downsam-
377 pled, in order to be able to compare the two results. The GM contributions
378 in the CBF maps obtained by applying the general kinetic model to the HR
379 perfusion and M0 images, without noise, were considered as the references
380 to which the generated images had to be compared. Figure 8 illustrates the
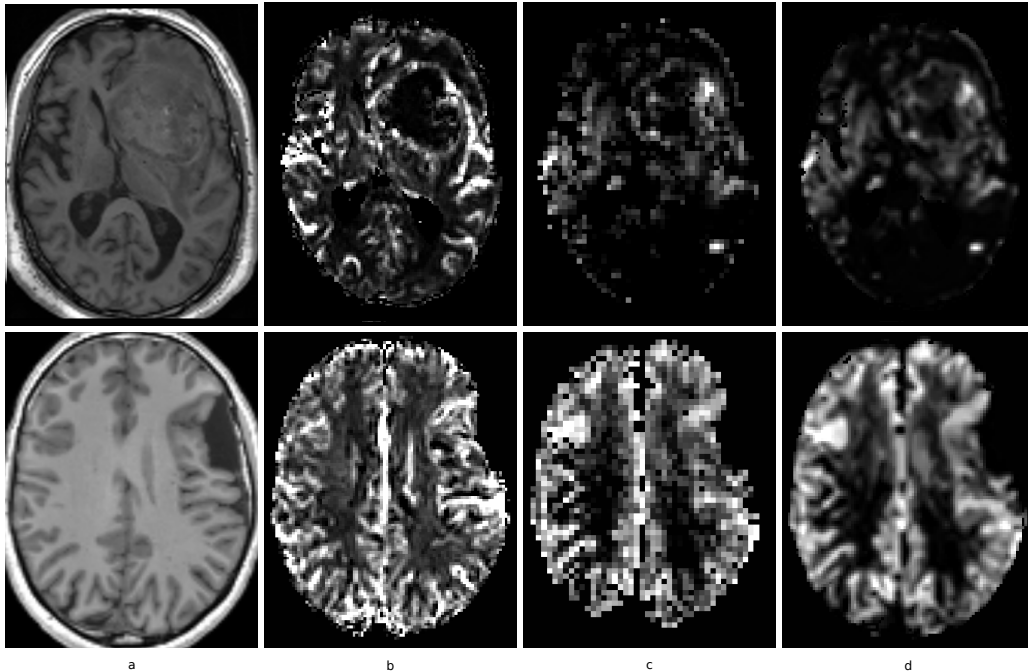381 pipeline that corresponds to the above-mentioned operations.

Figure 7: a) structural image, b) DSC CBF image, c) low resolution ASL CBF image and d) SR reconstructed ASL CBF map. The two lines correspond to images of two different subjects.

4.2. Results

Contrary to differences in the produced GM contribution maps reported in Zhao et al. [28], between an application of the linear regression to the calculated CBF map and to perfusion and M0 images before the CBF calculation, our method did not show such significant differences while testing for the influence of this effect. Figure 9 presents the GM contributions to the CBF values in a reference image, their recovery by application of the linear regression method to the low resolution CBF map, by applying the same method to perfusion and M0 images before CBF calculation, and after increasing the CBF image dimensions with our method. Figure 10 shows the difference images obtained after the subtraction of each of the produced images listed above and the corresponding reference. An important aspect illustrated in these difference images is the fact, already stated in [6, 7, 12, 28], that the linear regression method implies a smoothing of the GM contributions. On the contrary, the sinusoidal variations are retained in the image
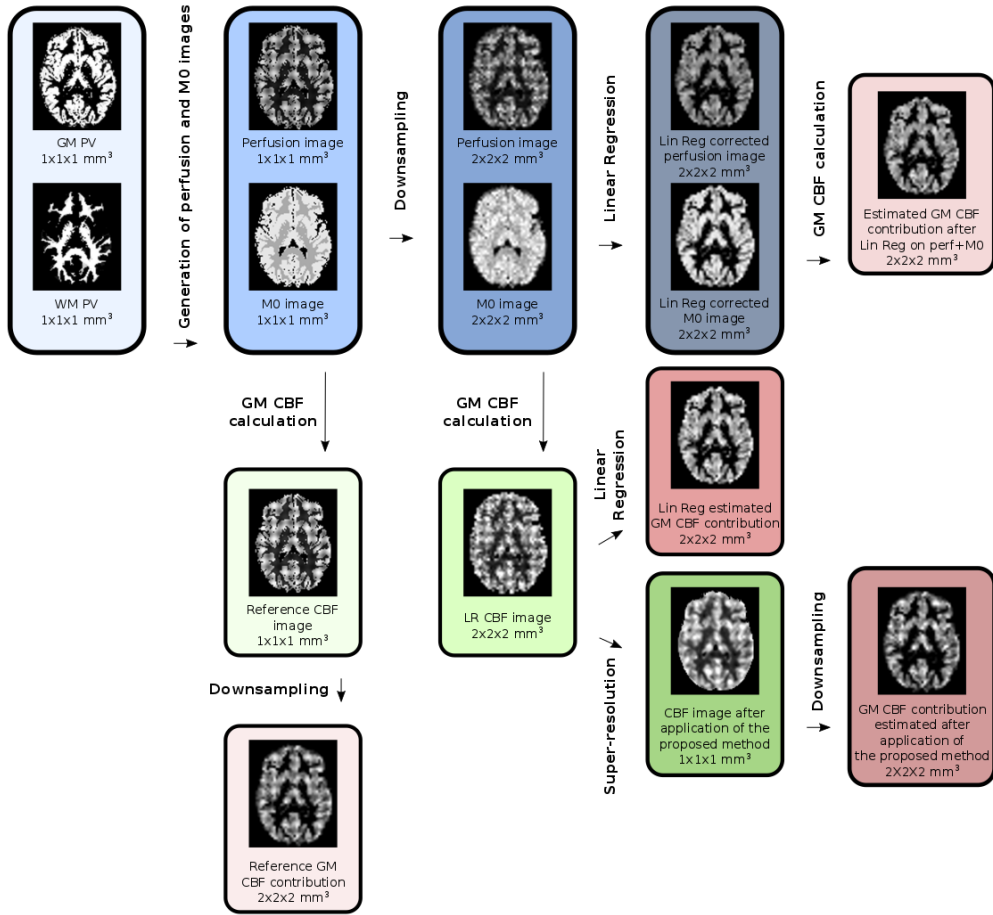
17

Figure 8: Pipeline describing the operations applied to each of the 9 images of the simulated dataset and the GM contribution assessment maps to be compared.

originating from the proposed algorithm.

Table 3 presents the evolution of the mean RMSE values calculated between the generated GM contribution images and their references as a function of noise (SNR=inf, 10, 5). In practice, both applications of the linear regression method to the CBF maps or to the perfusion and M0 images are commonly accepted [28]. Since the mean RMSE values obtained by applying our method to CBF maps are bounded by the mean RMSE provided by these two linear regressions, we can presume that our method reduces the influence of PVE. Moreover, the linear regression method is based on the use of information provided by partial volume estimates, which makes it dependent upon the

chosen segmentation algorithm and sensitive to potential segmentation errors. On the contrary, our SR reconstruction method is independent of any segmentation algorithm. In order to investigate the influence of these segmentation corruptions on the GM contribution maps resulting from the application of the linear regression, we simulated variations in the segmented partial volume estimates by introducing gaussian noise or by applying an opening and closing morphological operation to these partial volume maps. Tables 4 and 5 show a significant increase in the mean RMSE values when the partial volume estimates are modified. These results indicate that the property of the SR reconstruction to be independent of the use of partial volume estimates could be of great interest to avoid potential errors due to segmentation corruption.
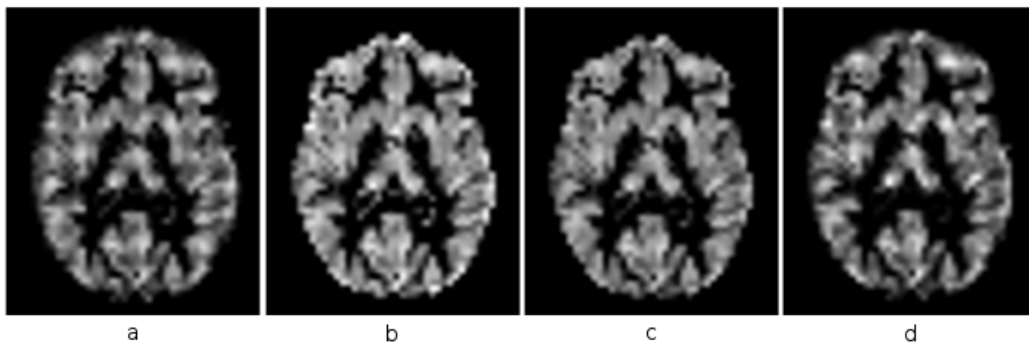

Figure 9: Comparison of gray matter cerebral blood flow contribution maps: a) GM contribution maps from the reference image, b) linear regression applied to the low resolution CBF image, c) linear regression applied to the low resolution perfusion and M0 images, and d) proposed SR method applied to the LR CBF image (SNR=5).

Method	SNR=inf	SNR=10	SNR=5
Lin Reg on CBF	6.41 ± 0.74	6.54 ± 0.75	7.05 ± 0.75
Lin Reg on Perf & M0	4.39 ± 0.17	4.52 ± 0.17	4.90 ± 0.17
SR on CBF	5.66 ± 0.11	5.94 ± 0.13	6.77 ± 0.14

Table 3: Mean RMSE values between the reference GM CBF contribution images and the images obtained after linear regression (Lin Reg) on the low resolution (LR) CBF image, Lin Reg on the perfusion and M0 images, and the proposed SR method applied to the LR CBF images.
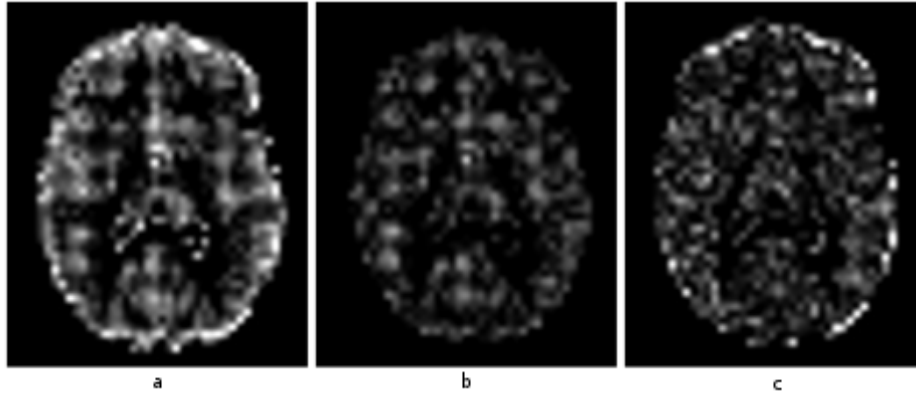
19

Figure 10: Comparison of gray matter cerebral blood flow contribution maps: a) difference images obtained by subtraction of the reference GM contribution map from the images obtained by applying the linear regression (Lin Reg) to the low resolution (LR) CBF image, b) the linear regression to the LR perfusion and M0 images, and c) the proposed SR method to the LR CBF image (SNR=5).

Method	SNR=inf	SNR=10	SNR=5
Lin Reg on CBF	7.46 ± 0.60	7.65 ± 0.59	8.09 ± 0.62
Lin Reg on Perf & M0	5.84 ± 0.23	5.97 ± 0.24	6.24 ± 0.22
SR on CBF	5.66 ± 0.11	5.94 ± 0.13	6.77 ± 0.14

Table 4: Mean RMSE values between the reference GM CBF contribution images and the images obtained after linear regression (Lin Reg) on the low resolution(LR) CBF image and on the perfusion and M0 images, with noise added to the partial volume estimates needed by the Lin Reg method, and the proposed SR method applied to the LR CBF images.

Method	SNR=inf	SNR=10	SNR=5
Lin Reg on CBF	11.68 ± 0.70	11.78 ± 0.70	12.10 ± 0.75
Lin Reg on Perf & M0	11.19 ± 0.50	11.23 ± 0.49	11.42 ± 0.51
SR on CBF	5.66 ± 0.11	5.94 ± 0.13	6.77 ± 0.14

Table 5: Mean RMSE values between the reference GM CBF contribution images and the images obtained after linear regression (Lin Reg) on the low resolution (LR) CBF image and on the perfusion and M0 images, with an opening+closing operation added to the partial volume estimates needed by the Lin Reg method, and the proposed SR method applied to the LR CBF images.

5. Discussion

In this work, we have presented and investigated different properties of a SR reconstruction method dedicated to ASL images. This method enables to

20

increase the level of details, while providing a denoising of the reconstructed images. It is based on the assumptions of an appearing accordance between neighborhoods in the image to be reconstructed and a classically acquired HR anatomical image, and that distant neighborhoods could serve as a learning database in the reconstruction process.

On a simulated dataset, we have shown that the contributions of the ASL and structural related terms can be considered as equivalent in the reconstruction process, by selecting $[\beta_{asl}; \beta_{struct}] = [0.5; 0.5]$. Our method is also shown to provide images closer to references than common interpolation techniques. The fact that this result could be obtained with different levels of noise added to the images to be reconstructed is an indication of the ability of the proposed method to denoise the reconstructed images.

Experiments on low resolution data acquired on healthy subjects confirmed these findings in 3 over 4 sujects. The main limitation of this study is nonetheless the relevance of the definition of the HR ASL images as references, because of their low SNR. In order to maintain the scan time reasonable and avoid subject motions that would almost certainly happen after 10 minutes of continuous scanning, 100 control-label repetitions have been acquired to generate the high resolution ASL images. This number is certainly still not sufficient to obtain an appropriate image quality, which could explain the fact that a better RMSE value was obtained by applying a 3rd order B-spline interpolation for the first subject. This limitation is precisely the reason why we chose to conduct the two other studies, meaning with a simulated dataset and the comparison with DSC images.

The study based on images of patients with brain tumors revealed a significantly increased correlation between DSC and images reconstructed with our method, supporting the capability of the proposed method to recover details by driving the reconstruction of ASL images with a high resolution structural one. The TI value chosen to acquire these PASL data was possibly a little short for subjects 5, 6 and 10, associated to intense ASL signals in their macrovasculature, which could explain the reduced correlation values obtained for these three subjects.

We showed that our method associates an increase in the level of details with a reduction of the partial volume effect in ASL images. The main advantage of this SR reconstruction in comparison with the linear regression partial volume correction method is to preserve spatial signal fluctuations, which are smoothed by the latter.

Despite the three validation approaches that were addressed in the context

21

of this work, we did not evaluate the method on pathologies implying subtle and localized perfusion changes. Investigating the capability of the method to preserve CBF modifications appearing before structural changes, as it is the case for early stages of neurodegenerative disease for exemple, would be of interest as a future work.

The method proposed in this paper only depends on the accurate registration of a HR structural image on the initially interpolated ASL image to be reconstructed. Indeed, experiments revealed that the initial interpolation method selected in order to increase the dimension of the image to reconstruct does not have a significant influence on the generated image, and denoising is performed jointly with the increase in the level of details. This aspect makes our method an appropriate tool to increase the quality and the fidelity of ASL images, and particularly CBF maps, with respect to effective physiological processes. Another promising aspect is its capability to recover well detailed ASL images from standard clinical acquisition protocols, therefore not increasing the acquisition time and patient discomfort. We believe that such a post-processing procedure could help clinicians to establish even more accurate diagnosis, by reducing interrogations concerning the reasons of reduced perfusion values and being able to distinguish GM thickness reduction or an effective perfusion reduction for example.

6. Acknowledgements

22

References

[1] J. A. Detre, H. Rao, D. J. Wang, Y. F. Chen, Z. Wang, Applications of arterial spin labeled MRI in the brain, Journal of Magnetic Resonance Imaging 35 (2012) 1026–1037.

[2] R. B. Buxton, L. R. Frank, E. C. Wong, B. Siewert, S. Warach, R. R. Edelman, A general kinetic model for quantitative perfusion imaging with arterial spin labeling, Magnetic Resonance in Medicine 40 (1998) 383–396.

[3] L. M. Parkes, P. S. Tofts, Improved accuracy of human cerebral blood perfusion measurements using arterial spin labeling: Accounting for capillary water permeability, Magnetic Resonance in Medicine 48 (2002) 27–41.

[4] D. C. Alsop, J. A. Detre, X. Golay, M. Gnther, J. Hendrikse, L. Hernandez-Garcia, H. Lu, B. J. MacIntosh, L. M. Parkes, M. Smits, M. J. P. van Osch, D. J. J. Wang, E. C. Wong, G. Zaharchuk, Recommended implementation of arterial spin-labeled perfusion mri for clinical applications: A consensus of the ismrm perfusion study group and the european consortium for asl in dementia, Magnetic Resonance in Medicine 73 (2015) 102–116.

[5] P. M. Figueiredo, S. Clare, P. Jezzard, Quantitative perfusion measurements using pulsed arterial spin labeling: Effects of large region-of-interest analysis, Journal of Magnetic Resonance Imaging 21 (2005) 676–682.

[6] I. Asllani, A. Borogovac, T. R. Brown, Regression algorithm correcting for partial volume effects in arterial spin labeling mri, Magnetic Resonance in Medicine 60 (2008) 1362–1371.

[7] M. A. Chappell, A. R. Groves, B. J. MacIntosh, M. J. Donahue, P. Jezzard, M. W. Woolrich, Partial volume correction of multiple inversion time arterial spin labeling mri data, Magnetic Resonance in Medicine 65 (2011) 1173–1183.

[8] C. Maumet, P. Maurel, J.-C. Ferr, C. Barillot, Robust estimation of the cerebral blood flow in arterial spin labelling, Magnetic Resonance Imaging 32 (2014) 497 – 504.

23

[9] J. Petr, J.-C. Ferre, J.-Y. Gauvrit, C. Barillot, Improving arterial spin labeling data by temporal filtering, Proc.SPIE 7623 (2010) 7623 – 7623 – 9.

[10] A. Buades, B. Coll, J. M. Morel, A review of image denoising algorithms, with a new one, Multiscale Modeling & Simulation 4 (2005) 490–530.

[11] P. Coupe, P. Yger, S. Prima, P. Hellier, C. Kervrann, C. Barillot, An optimized blockwise nonlocal means denoising filter for 3-d magnetic resonance images, IEEE Transactions on Medical Imaging 27 (2008) 425441.

[12] J. Petr, J.-C. Ferre, J.-Y. Gauvrit, C. Barillot, Denoising arterial spin labeling mri using tissue partial volume, Proc.SPIE 7623 (2010) 7623 – 7623 – 9.

[13] B. Scherrer, A. Gholipour, S. K. Warfield, Super-resolution reconstruction to increase the spatial resolution of diffusion weighted images from orthogonal anisotropic acquisitions, Medical Image Analysis 16 (2012) 1465–1476.

[14] F. Rousseau, A non-local approach for image super-resolution using intermodality priors, Medical Image Analysis 14 (2010) 594–605.

[15] J. V. Manjón, P. Coupé, A. Buades, D. L. Collins, M. Robles, MRI superresolution using self-similarity and image priors, International Journal of Biomedical Imaging 2010 (2010) 1–11.

[16] P. Coupé, J. V. Manjón, M. Chamberland, M. Descoteaux, B. Hiba, Collaborative patch-based super-resolution for diffusion-weighted images, NeuroImage 83 (2013) 245–261.

[17] M. Protter, M. Elad, H. Takeda, P. Milanfar, Generalizing the nonlocal-means to super-resolution reconstruction, IEEE Transactions on Image Processing 18 (2009) 36–51.

[18] C. Meurée, P. Maurel, C. Barillot, Patch-based super-resolution for arterial spin labeling MRI , ISMRM 25th Annual Meeting & Exhibition (2017).

[19] J. P. Marques, T. Kober, G. Krueger, W. van der Zwaag, P.-F. V. de Moortele, R. Gruetter, MP2rage, a self bias-field corrected sequence for improved segmentation and t1-mapping at high field, NeuroImage 49 (2010) 1271–1281.

[20] L. M. Parkes, W. Rashid, D. T. Chard, P. S. Tofts, Normal cerebral perfusion measurements using arterial spin labeling: Reproducibility, stability, and age and gender effects, Magnetic Resonance in Medicine 51 (2004) 736–743.

[21] Statistical Parametric Mapping: The Analysis of Functional Brain Images, Academic Press, 2006.

[22] W.-C. Wu, M. Fernández-Seara, J. A. Detre, F. W. Wehrli, J. Wang, A theoretical and experimental investigation of the tagging efficiency of pseudocontinuous arterial spin labeling, Magnetic Resonance in Medicine 58 (2007) 1020–1027.

[23] L. Østergaard, R. M. Weisskoff, D. A. Chesler, C. Gyldensted, B. R. Rosen, High resolution measurement of cerebral blood flow using intravascular tracer bolus passages. part i: Mathematical approach and statistical analysis, Magnetic Resonance in Medicine 36 (1996) 715–725.

[24] C. Warmuth, M. Günther, C. Zimmer, Quantification of blood flow in brain tumors: Comparison of arterial spin labeling and dynamic susceptibility-weighted contrast-enhanced MR imaging, Radiology 228 (2003) 523–532.

[25] H. Ma, Z. Wang, K. Xu, Z. Shao, C. Yang, P. Xu, X. Liu, C. Hu, X. Lu, Y. Rong, Three-dimensional arterial spin labeling imaging and dynamic susceptibility contrast perfusion-weighted imaging value in diagnosing glioma grade prior to surgery, Experimental and Therapeutic Medicine 13 (2017) 2691–2698.

[26] L. Knutsson, D. van Westen, E. T. Petersen, K. M. Bloch, S. Holtås, F. Ståhlberg, R. Wirestam, Absolute quantification of cerebral blood flow: correlation between dynamic susceptibility contrast MRI and model-free arterial spin labeling, Magnetic Resonance Imaging 28 (2010) 1–7.

[27] K. Gorgolewski, C. D. Burns, C. Madison, D. Clark, Y. O. Halchenko, M. L. Waskom, S. S. Ghosh, Nipype: A flexible, lightweight and extensible neuroimaging data processing framework in python, Frontiers in Neuroinformatics 5 (2011).

[28] M. Y. Zhao, M. Mezue, A. R. Segerdahl, T. W. Okell, I. Tracey, Y. Xiao, M. A. Chappell, A systematic study of the sensitivity of partial volume correction methods for the quantification of perfusion from pseudo-continuous arterial spin labeling MRI, NeuroImage 162 (2017) 384–397.